DOI: 10.5075/epfl-ICSS12-2018-133-135

2D QUASI-STATIC DELAMINATION IN GFRP LAMINATES: NUMERICAL INVESTIGATION

Aida Cameselle-Molares[1], Anastasios P. Vassilopoulos[1], Jordi Renart[2], Albert Turon[2] and Thomas Keller[1]
[1]Composite Construction Laboratory (CCLab), École Polytechnique Fédérale de Lausanne (EPFL), Switzerland.
aida.camesellemolares@epfl.ch, anastasios.vasilopoulos@epfl.ch, thomas.keller@epfl.ch
[2]AMADE, Mechanical Engineering and Industrial Construction Department, Universitat de Girona, Spain.
jordi.renart@udg.edu, albert.turon@udg.edu

1. INTRODUCTION

Delamination in laminated components is one of the most critical types of damage. Thus, significant efforts have been devoted to investigate delamination in laminated composites [1], mostly in beam-like specimens, which have been widely investigated and standardized [2]. However, some of the conditions required by these types of experiments (e.g. constant crack width or single direction of propagation) may not correspond to the actual damage growth in FRP structures where delamination may develop all around the contour of a defect.

The experimental fracture behavior of laminated FRP plates with an embedded circular pre-crack (i.e. 2D delamination) and subjected to quasi-static out-of-plane opening loads is presented in another abstract of this conference [3]. This abstract focuses on the numerical investigation of the 2D in-plane crack propagation in two of these laminated plates. To compare and to understand the transition from standard 1D fracture experiments to 2D crack propagation scenarios, DCB specimens were further experimentally and numerically investigated.

2. EXPERIMENTAL METHODS, RESULTS AND DISCUSSION

Experimental Investigation of Laminated Plates

The 2D delamination behavior of GFRP laminated plates under quasi-static out-of-plane opening loading was experimentally investigated and presented in [3]. The experimental results obtained for the two laminated plates studied here (with long continuous filament reinforcement, CFM) are summarized in Fig. 1, where the load vs displacement and average crack-length vs displacement curves are shown for both CFM plates (Fig. 1(a)). Likewise, the curves illustrating the crack area vs the compliance of the plates are shown in Fig. 1(b). The minimum value in these curves (changing from decreasing to increasing behavior) was named “transition point” (TP) (see [3]).

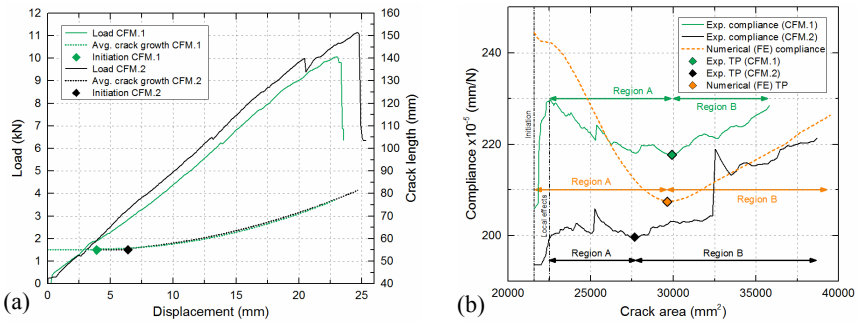

Fig. 1: (a) Experimental load and crack length vs displacement curves and (b) Comparison of experimental and numerical crack area vs compliance of CFM plates.

Experimental Investigation of Mode I DCB Specimens

Double cantilever beam specimens were used to determine the Mode I strain energy release rate (SERR). The same material system and lay-up (6 layers of CFM) as those of the plates were used. A Teflon film was placed at the midplane to introduce the pre-cracks. Specimens of 250-mm length and of different widths (25, 40, 60 and 100 mm) were investigated.

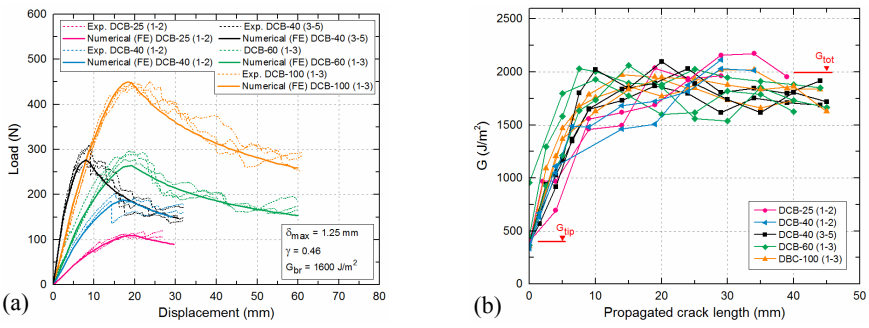

Fig. 2: (a) Comparison of experimental and numerical load-displacement curves; (b) experimental R-curves.

The experimental load-displacement responses of DCB specimens are shown in Fig. 2(a) and the experimental R-curves in Fig. 2(b). The total SERR, G_{tot}, derived from the experiments is the sum of the SERR at the crack tip, G_{tip}, and the SERR due to the fiber-bridging, G_{br}. According to these curves, values of 400 and 2000 J/m^2 respectively were assigned to G_{tip} and G_{tot}. A value of ~10 mm for the fiber-bridging length was obtained along with a maximum crack-opening displacement (COD), δ_f, of ~1.25 mm. Similar R-curves were obtained independently of the specimens' width.

NUMERICAL METHODS, RESULTS AND DISCUSSION

Cohesive Zone Modeling

The type of traction-separation law used to define the behavior of the cohesive elements is shown in Fig. 3(a). The first part of the law (orange) is attributed to the initial damage and the area equals SERR at the crack tip, G_{tip} (i.e. the energy required for crack initiation). The second part (blue) corresponds to the SERR due to the fiber-bridging, G_{br}. Details of the formulation can be found in [4].

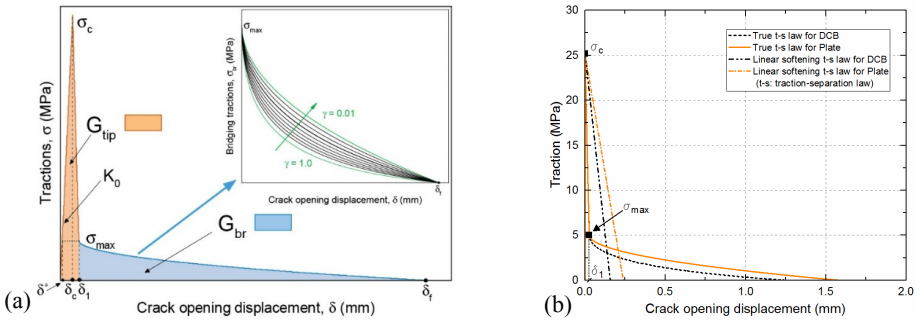

Fig. 3: Traction-separation curves; (a) general description and (b) used in numerical models.

Numerical Investigation of Mode I DCB Specimens

A finite element (FE) model was developed to simulate the delamination behavior of the DCB experiments using the commercial analysis software ABAQUS 6.14.1. The two GFRP beams were modeled with 3D built-in continuum shell elements and a single zero-thickness layer of three-dimensional cohesive elements was implemented at the midplane in the un-cracked region. Further details concerning this FE model can be found in [4]. The experimentally obtained SERR values of G_{tip}=400 J/m^2 and G_{tot}=2000 J/m^2 (i.e. G_{br}=1600 J/m^2) and the maximum COD (δ_f =1.25 mm) were assigned. The maximum traction for damage initiation was assumed to be equal to 30% of the tensile strength of the matrix, i.e. σ_c =25.2 MPa. The initial cohesive stiffness, K_0, was taken as being equal to 10^5 MPa/mm. The values of the maximum bridging traction, σ_{max}, and the bridging traction decay ratio, γ, were estimated iteratively. Corresponding values of 5 MPa and 0.46 were obtained. The resulting traction-separation law is presented in Fig. 3(b). The obtained numerical load-displacement curves (in good agreement with the experimental ones) are shown in Fig. 3(a).

Numerical Investigation of Laminated Plates

For the simulation of the CFM plates ABAQUS 6.14.1 was also employed. The FE model is described in Fig. 4.

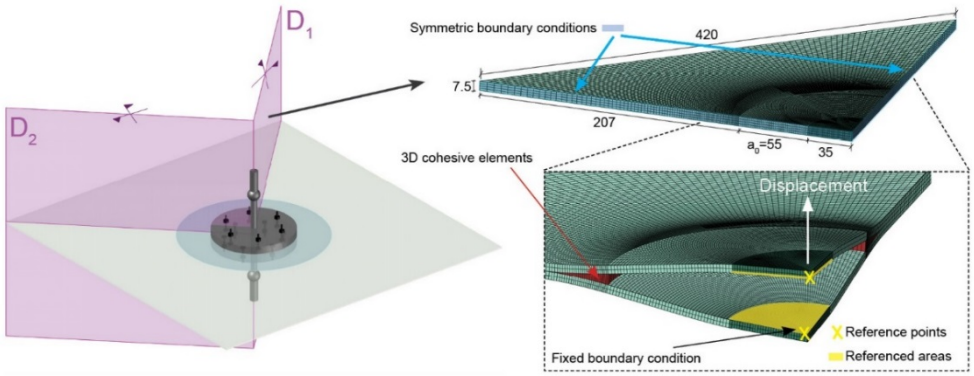

Fig. 4: Description of finite element model of laminated plate.

The built-in continuum shell element of eight nodes from Abaqus/Standard was used to mesh the bulk material. Two through-thickness elements were assigned to each of the halves of the plate. A single zero-thickness layer of 3D cohesive elements of eight nodes was implemented at the midplane of the un-cracked region. Further details of the model can be found in [4].

Initially, the same traction-separation law obtained for the DCB specimens was used (Fig. 3(b)), the total value of the SERR being therefore equal to G_{tot} =2000 J/m^2. However, the numerical load-displacement response obtained with these values did not correspond to the experimental curves, as shown in Fig. 5(a).

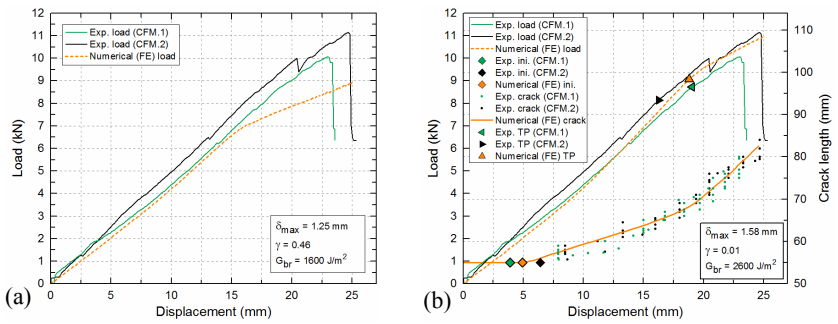

Fig. 5: Comparison of experimental and numerical results of CFM plates; (a) load-displacement curves using cohesive parameters and G_{tot} from DCBs and (b) load and crack length vs opening displacement curves with the adjusted parameters.

To better approach the experimental behavior, a fitting process was carried out. The values of K_0, G_{tip}, σ_c and σ_{max} (matrix-dominated values) were kept constant and the same as those obtained from the DCB specimens. The adjustment of the law was accomplished by fitting the value of G_{br} and therefore modifying the values of γ and δ_f. The values that allowed the FE model to approach the experimental behavior were γ = 0.01 and δ_f =1.58 mm, which lead to a G_{br} value of 2600 J/m^2 and therefore to a G_{tot} value of 3000 J/m^2 (see Fig. 3(b)). The revised numerical load-displacement and crack length-displacement curves are shown in Fig. 5(b). The numerical compliance vs crack area is shown in Fig. 1(b).

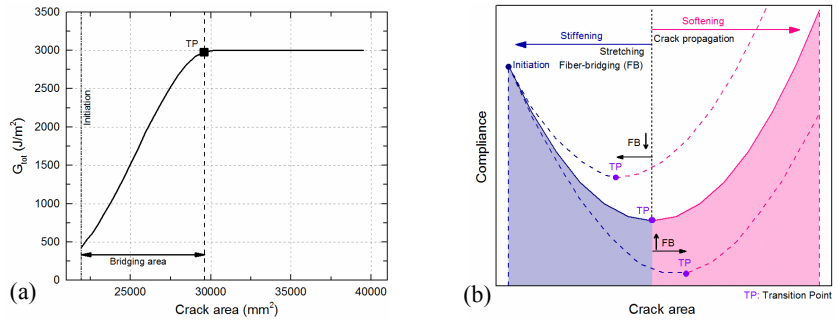

Fig. 6: (a) Numerical R-curve of laminated plate; (b) description of general behavior of crack area vs compliance curves.

The numerical value of the crack area at the TP in Fig. 1(b) coincides with the numerical value of the fully developed bridging area in the numerical R-curve (Fig. 6(a)). Consequently, with the value of the area at the TP obtained from the compliance vs crack area curve, the value of the bridging area can be directly obtained (here ~29600 mm^2 corresponding to a propagated radial length of ~13.2 mm). As a result, any decrease or increase in the bridging area would lead the compliance vs crack area curve moving to the left or right respectively (Fig. 6(b)).

The total value of the SERR obtained from the FEM of the plates was 50% higher than the total SERR derived from the DCB specimens (2000 vs 3000 J/m^2). This increase in the G_{tot} was directly related to the difference in stiffness between the DCB specimens and the plates. Furthermore, the stretching of the deformed part of the plate resulted in a "stress stiffening" effect. Consequently, more fiber-bridging than in the DCB specimens developed in the plates.

CONCLUSIONS

A numerical investigation of the 2D crack propagation in laminated plates was carried out to simulate the fracture behavior of the same plates that were previously experimentally investigated [3]. Additional DCB experiments were performed to study the transition from 1D to 2D crack propagation scenarios. The following conclusions can be drawn:

1. The selected shape of the traction-separation law was able to model the fracture behavior of the plates.
2. The stress stiffening of the plates and the increase in the flexural stiffness led to an increase of the fiber-bridging area, causing a 50% increase of the total SERR compared to the total SERR obtained from the DCB specimens.
3. The fully developed fiber-bridging area in the plates was correlated with the crack area at the transition point of the compliance vs crack area curves.

REFERENCES

[1] A.J. Brunner, "Experimental aspects of Mode I and Mode II fracture toughness testing of fiber-reinforced polymer-matrix composites", *Comput. Methods Appl. Mechs. Eng.*, 2000; 185: 161-172.

[2] ASTM D5528-13: Standard test method for mode I interlaminar fracture toughness for unidirectional fiber-reinforced polymer matrix composites, in Annual book of ATM standards: adhesive section 15.03.

[3] A. Cameselle-Molares et al., "2D quasi-static delamination in GFRP laminates: experimental investigation", *Extended abstract in the 12th International Conference in Sandwich Structures (ICSS12)*, 2018; 19-22 August, Lausanne, Switzerland.

[4] A. Cameselle-Molares et al., "Numerical simulation of two-dimensional in-plane crack propagation in FRP laminates", *Compos. Struct.*, 2018; 200:396-407